NETWORKS AND HETEROGENEOUS MEDIA
©American Institute of Mathematical Sciences
Volume **12**, Number **4**, December **2017**
doi:10.3934/nhm.2017025
pp. **619–642**

A MULTISCALE MODEL REDUCTION METHOD FOR NONLINEAR MONOTONE ELLIPTIC EQUATIONS IN HETEROGENEOUS MEDIA

Eric Chung

Department of Mathematics
The Chinese University of Hong Kong
Hong Kong, SAR, China

Yalchin Efendiev[1], Ke Shi[2] and Shuai Ye[1]

[1]Department of Mathematics
Texas A & M University
College Station, TX 77843, USA
[2]Department of Mathematics & Statistics
Old Dominion University
Norfolk, VA 23529, USA

(Communicated by Claude Le Bris)

Abstract. In this paper, we present a multiscale model reduction framework within Generalized Multiscale Finite Element Method (GMsFEM) for nonlinear elliptic problems. We consider an exemplary problem, which consists of nonlinear p-Laplacian with heterogeneous coefficients. The main challenging feature of this problem is that local subgrid models are nonlinear involving the gradient of the solution (e.g., in the case of scale separation, when using homogenization). Our main objective is to develop snapshots and local spectral problems, which are the main ingredients of GMsFEM, for these problems. Our contributions can be summarized as follows. (1) We re-cast the multiscale model reduction problem onto the boundaries of coarse cells. This is important and allows capturing separable scales as discussed. (2) We introduce nonlinear eigenvalue problems in the snapshot space for these nonlinear "harmonic" functions. (3) We present convergence analysis and numerical results, which show that our approaches can recover the fine-scale solution with a few degrees of freedom. The proposed methods can, in general, be used for more general nonlinear problems, where one needs nonlinear local spectral decomposition.

1. Introduction.

Many processes in nature have multiscale nature and nonlinearities. The interaction between nonlinearities and multiple scales can be complex and non separable. This occurs in many applications. A specific feature for this non-separability

2010 *Mathematics Subject Classification.* Primary: 65N99.

Key words and phrases. Generalized Multiscale Finite Element method, multiscale, nonlinear monotone elliptic problem, p-Laplacian, high-contrast.

Eric Chung would like to thank the partial support of the CUHK Direct Grant for Research 2015/16 and the Hong Kong RGC General Research Fund (Project: 14317516). YE would like to thank the partial support from NSF 1620318, the U.S. Department of Energy Office of Science, Office of Advanced Scientific Computing Research, Applied Mathematics program under Award Number DE-FG02-13ER26165, the mega-grant of the Russian Federation Government (N 14.Y26.31.0013), and National Priorities Research Program grant NPRP grant 7-1482-1278 from the Qatar National Research Fund.

is that nonlinearities change the multiscale nature of the solution. To discuss some main concepts, we consider an example

$$div(a(x,u,\nabla u)) = f. \tag{1}$$

We assume $a(x,\cdot,\cdot)$ is highly heterogeneous with respect to x. From the point of view of the interaction between nonlinearities and the multiple scales, one can distinguish several classes. In some nonlinear problems, the nonlinearities within coarse regions (a computational grid), that induce the change in the heterogeneities, can be parametrized with a low dimensional parameter, e.g., $a(x,u,\nabla u) = a_0(x,u)\nabla u$ (assuming smoothness and boundedness of a). Within each coarse region, one can approximate the solution u by a constant and thus, can handle these nonlinearities via a low dimensional parametrization (see, e.g., [30, 46] for homogenization and numerical homogenization discussions). If the nonlinearities and heterogeneities are separable in this case, i.e., $a(x,u,\nabla u) = a(x)b(u)\nabla u$, then, in fact, one can use a linear theory of multiscale methods (cf. [30, 46]). The situation is very different when $a(x,u,\nabla u) = a_1(x,\nabla u)\nabla u$. Because ∇u is highly heterogeneous, one can not use any low dimensional approximation and linear theories (see e.g., [30, 46, 37, 36, 13, 3, 42, 44] for homogenization and numerical homogenization). This is true even for a separable case $a(x,u,\nabla u) = a_0(x)b(|\nabla u|)\nabla u$. These problems require nonlinear cell problems ([30, 46, 37, 36, 13, 3, 42, 44]). In the paper, we focus on $a(x,u,\nabla u) = a(x,\nabla u)$ and discuss these nonlinear cell problems for GMsFEM.

Many previous research on multiscale methods have considered nonlinear problems. The approaches including homogenization [47, 41], numerical homogenization [2, 49, 21], heterogeneous multiscale methods [22, 1, 37, 43], multiscale network approximations [8, 9, 7], multiscale finite element methods [21, 49, 4, 27, 24, 28, 34, 33, 23, 25, 29, 14], variational multiscale methods [39, 38, 6, 40], polyharmonic homogenization [45, 10], generalized multiscale finite element methods [24, 26, 11, 18, 16, 17] have been developed and applied. These approaches approximate the solution of nonlinear PDEs on a coarse grid (see Figure 1 for illustration of coarse and fine grids) by using subgrid models. Some common ingredients in these methods for linear problems are that local solutions are calculated and used to form equations on a coarse grid. GMsFEM approaches propose a systematic enrichment, which calculates multiscale basis functions via local spectral decomposition in each coarse cell. The extensions of these methods to nonlinear problems (as (1)) use nonlinear local problems. For example, in numerical homogenization methods, one can use as a local problem in each coarse cell, for the case $a(x,u,\nabla u) = a(x,\nabla u)$,

$$-div(a(x,\nabla\phi_\xi)) = 0$$

with the boundary conditions $\phi = \xi \cdot x$. The homogenized fluxes are computed by averaging the flux $a^*(\xi) = \langle a(x,\nabla\phi_\xi)\rangle$. These approaches follow homogenization theory ([46, 37, 36, 13, 3, 42, 44], see also [1, 37, 43] and, the references therein, for numerical homogenization), which is well developed. For GMsFEM, a systematic local enrichment via appropriate local nonlinear spectral problems is needed.

The main idea of GMsFEM for linear problems is to form snapshot spaces and perform local spectral decomposition in the snapshot space. In this paper, we will follow the same general concept and introduce nonlinear eigenvalue problems. Previous approach [31] develops local nonlinear eigenvalue problems in each coarse cell. Our main contribution is the development of a systematic model reduction using nonlinear harmonic functions. The latter is important as it allows capturing the effects of separable scales. Without using nonlinear harmonic functions, one can not, in general, capture

the effects of small separable scales. This is in contrast to linear problems, where one can construct one linear basis function per every coarse node that contains the effects of small scales. Using local solutions allows compressing the effects of small scales within a coarse block and we work with a system reduced to the boundaries of coarse cells. In this case, we can also guarantee that our approaches recover homogenization results when there is a scale separation (note that previous approaches [31] can not guarantee it). The proposed method is in a spirit of hybridization techniques [20, 32, 15] and necessary to eliminate the scale interactions in each block.

In the paper, we present a local enrichment procedure for the degrees of freedom defined on the boundaries. Our computations are performed in a nonlinear space, where any function defined on the boundaries of coarse cells is extended harmonically to the interior by using local nonlinear PDEs. Our snapshot space can be thought as a nonlinear map from the boundaries to the interior. We discuss the use of nonlinear eigenvalue problems, which are motivated by the analysis. Our analysis allows removing some of major assumptions that are used when not using local nonlinear-harmonic functions (see [31]).

The numerical results are presented for several examples. We consider a high-contrast permeability field in p-Laplacian example with heterogeneous coefficients. The high-contrast permeability field contains several channels and inclusions with a high permeability. In our numerical results, we increase the number of local multiscale basis functions and compute the errors. The results show that the error decreases rapidly as we increase the number of basis functions and we can approximate the global solution accurately with a very few degrees of freedom.

The paper is organized as follows. In Section 2, we present some preliminaries and also present a motivation. The description of the GMsFEM for nonlinear problem is presented in Section 3. The convergence analysis of the method is given in Section 4. We present numerical results in Section 5. The conclusion is drawn in Section 6.

2. Preliminaries and motivation.

2.1. Preliminaries and notations.

Let D be a bounded open set in $\mathbb{R}^2$ with Lipschitz boundary ∂D. We consider the following heterogeneous p-Laplacian equation

$$-div(a(x,\nabla u)) = f(x) \quad \text{in } D, \qquad u = g \quad \text{on } \partial D, \tag{2}$$

where $a(x,\nabla u) = \kappa(x)|\nabla u|^{p-2}\nabla u$, $p \geq 2$, $\kappa(x) \geq \kappa_0 > 0$ is a high-contrast coefficient (i.e., $\kappa_{\max}/\kappa_{\min}$ is large), $f \in W^{-1,q}(D)$ $(1/p + 1/q = 1)$ is an external forcing term, and $g \in W^{1/q,p}(D)$ is the Dirichlet boundary data.

The corresponding weak formulation is: $(\mathcal{P})$ Find $u \in W_g^{1,p}(D) \equiv \{v \in W^{1,p}(D) : v = g \text{ on } \partial D\}$ such that

$$\int_D a(x,\nabla u)\cdot\nabla v = \int_D fv, \qquad \forall v \in W_0^{1,p}(D).$$

The well-posedness of $(\mathcal{P})$ is well established, and one can refer to, for example, Glowinski and Marrocco [35] or the account in Ciarlet [19]. Throughout the paper, we define the energy norm of $u \in W^{1,p}(D)$ as

$$\|u\|_{1,p(D)} = \left(\int_D \kappa(x)|\nabla u|^p dx\right)^{1/p}.$$

Next, we describe the finite element approximation of the solution. We let $\mathcal{T}^h$ be a fine triangulation, and denote by $V^h = V^h(D)$ the usual finite element space

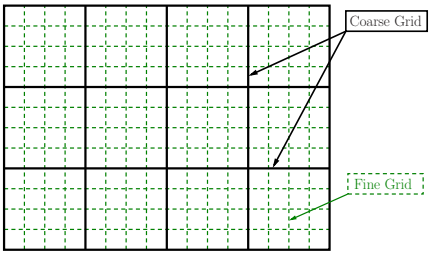

FIGURE 1. Illustration of a multiscale discretization

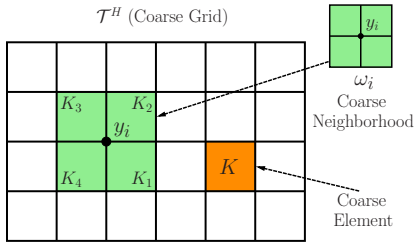

FIGURE 2. Illustration of a coarse neighborhood and elements

containing continuous piecewise linear functions with respect to $\mathcal{T}^h$. We also let $V_0^h(D)$ be the subset of $V^h(D)$ containing functions that vanish on ∂D. Similar notations, $V^h(\Omega), V_0^h(\Omega)$, are used for $\Omega \subset D$.

The discrete fine-scale problem is defined in the following: $(\mathcal{P}^h)$ Find $u^h \in V^h(D)$ such that

$$\int_D a(x, \nabla u^h) \cdot \nabla v = \int_D fv, \qquad \forall v \in V_0^h(D).$$

Additionally, we introduce a coarse discretization $\mathcal{T}^H$ in which each coarse element is comprised of a localized fine mesh. See Figure 1 for an illustration of a multiscale discretization containing both fine and coarse elements. We use $\{y_i\}_{i=1}^{N_v}$ to denote the vertices of the coarse mesh, and define a coarse neighborhood of y_i by

$$\omega_i = \bigcup \{K_j \in \mathcal{T}^H;\ y_i \in \overline{K}_j\}, \tag{3}$$

where K_j denotes a coarse element in the domain and N_v is the number of coarse vertices. See Figure 2 for an illustration of a coarse neighborhood and elements. Inside each coarse neighborhood ω_i $(i = 1, \cdots, N_v)$, we call the collection of the coarse edges with y_i being a common vertex the *cross* of y_i.

2.2. **Motivation.** First, we introduce the concept of *p-harmonic extension*.

Definition 2.1. Let $u \in W^{1,p}(K)$ $(p \geq 2)$ be a given function. Let $\tilde{u} \in W^{1,p}(K)$ be defined so that $\tilde{u} - u \in W_0^{1,p}(K)$, and that $\tilde{u}$ satisfies:

$$-div(a(x, \nabla \tilde{u})) = 0 \quad \text{in } K,$$

where $a(x, \nabla \tilde{u}) = \kappa(x)|\nabla \tilde{u}|^{p-2}\nabla \tilde{u}$. Then $\tilde{u}$ is called the *p-harmonic extension* of u. We denote $\tilde{u} := H_p(u)$.

Remark 1. The p-harmonic extension minimizes the energy norm, i.e.

$$\int_K \kappa(x)|\nabla \tilde{u}|^p dx = \min_{v \in W_u^{1,p}(K)} \int_K \kappa(x)|\nabla v|^p dx,$$

where $W_u^{1,p}(K) = \{v \in W^{1,p}(K) \,|\, v = u \text{ on } \partial K\}$.

Remark 2. In this context, all p-harmonic extensions are accomplished coarse-element by coarse-element. Though, we might use the notation H_p directly on a larger domain such as a coarse neighborhoods ω_i or the whole domain D, it means that the p-harmonic extension is performed on each coarse element contained in ω_i or D.

Our main idea is solving for the Generalized Multiscale Finite Element solution of Equation (2) on the *crosses* of the coarse mesh and then the solution in the whole domain can be approximated by p-harmonically extending the obtained cross values into the domain. This idea is motivated by the technique of Numerical Homogenization (NH), which is described in the following. Our goal is to show that our proposed Generalized Multiscale Finite Element Method recovers NH.

2.2.1. *Numerical Homogenization(NH) and Generalized Multiscale Finite Element.* First, we describe a well known numerical homogenization technique. This method can be regarded as using a limited number of degrees of freedom per coarse element. Our objective is to show that the numerical homogenization is a finite element approximation on a coarse grid using p-harmonic extension with only one degree of freedom per edge. We consider

$$-div(a(x,\nabla u)) = f \quad \text{in } D,$$

with $u = 0$ on ∂D. We consider a coarse-grid block K and our goal for each coarse-grid block is to compute the effective property. This is done by solving local problem

$$-div(a(x,\nabla N_\xi)) = 0 \quad \text{in } K,$$

with boundary condition $N_\xi = \xi \cdot x$ on ∂K. According to the previous definition, we can write $N_\xi = H_p(\xi \cdot x)$. Then $a^*(\cdot)$ is defined as

$$a^*(\xi) = \frac{1}{|K|}\int_K a(y,\nabla N_\xi)dy.$$

The coarse-grid equation is given by

$$-div(a^*(x,\nabla u^*)) = f \quad \text{in } D,$$

with $u^* = 0$ on ∂D. Suppose $u^* = \sum c_k\phi_k$, where $\{\phi_k\}$ is a linear basis, then

$$\begin{aligned} F^{NH}(\vec{c}) &= \int_D a^*(x,\nabla\sum c_k\phi_k)\cdot\nabla\phi_j dx \\ &= \sum_{K\in D}\int_K a^*(\sum c_k\nabla\phi_k)\cdot\nabla\phi_j dx, \end{aligned}$$

At this step, we denote $\sum c_k\nabla\phi_k = \xi = constant$, then $N_\xi = H_p(\sum c_k\nabla\phi_k\cdot x)$ and

$$\begin{aligned} F^{NH}(\vec{c}) &= \sum_{K\in D}\int_K a^*(\xi)\cdot\nabla\phi_j dx \\ &= \sum_{K\in D}\int_K\left(\frac{1}{|K|}\int_K a(x,\nabla N_\xi)dx\right)\cdot\nabla\phi_j dx \\ &= \int_D\frac{1}{|K|}\left(\int_K a(x,\nabla H_p(\sum c_k\nabla\phi_k\cdot x))dx\right)\cdot\nabla\phi_j dx \\ &= \int_D\frac{1}{|K|}\left(\int_K a(x,\nabla H_p(\sum c_k\phi_k))dx\right)\cdot\nabla\phi_j dx \\ &= \int_D f\phi_j dx. \end{aligned}$$

Compared with the numerical homogenization, Generalized Multiscale Finite Element method seeks the approximation of the solution in the form $\sum_{i,k}\chi_i c_k^{\omega_i}\phi_k^{\omega_i}$, which

solves

$$F(\vec{c}) = \int_D a(x, \nabla H_p(\sum_{i,k} \chi_i c_k^{\omega_i} \phi_k^{\omega_i}) \cdot \nabla \phi_j^{\omega_i} dx$$
$$= \int_D f \phi_j^{\omega_i} dx,$$

where $\{\phi_k^{\omega_i}\}_{k=1}^{L_i}$ (L_i is the number of basis chosen in ω_i) are generalized multiscale basis constructed in each ω_i ($i = 1, \cdots, N_v$), $\{\chi_i\}_{i=1}^{N_v}$ is the set of partition of unity functions. Our main approach is to construct multiscale basis functions in a systematic way and provide a priori error. We see from the above discussion that Generalized Multiscale Finite Element Method can be thought as an extension of Numerical Homogenization, where we need to identify appropriate procedures for finding multiscale basis functions. In the following section, we will describe the details of constructing multiscale basis as well as partition of unity functions.

3. **Generalized multiscale finite element method.** The goal of our proposed generalized multiscale finite element method is to find a numerical approximation of the solution as well as employing the degree of freedoms only on the crosses in order to exhibit model reduction. Suppose the generalized multiscale finite element solution we are seeking for is $u_{ms} = H_p(\sum_i \sum_{k=1}^{L_i} \chi_i c_k^{\omega_i} \phi_k^{\omega_i})$, where $\{\phi_k^{\omega_i}\}_{k=1}^{L_i}$ are multiscale basis constructed in each coarse neighborhood ω_i, $\{\chi_i\}_{i=1}^{N_v}$ is the set of partition of unity functions, then the generalized multiscale finite element formulation for Equation (2) is the following: Find $\vec{c} = \{c_k^{\omega_i}\}_{i,k}$ such that

$$\int_D a(x, \nabla H_p(\sum_i \sum_{k=1}^{L_i} \chi_i c_k^{\omega_i} \phi_k^{\omega_i}) \cdot \nabla \phi_j^{\omega_i} dx = \int_D f \phi_j^{\omega_i} dx \qquad \text{for any } j, \tag{4}$$

where $a(x, \nabla u) = \kappa(x) |\nabla u|^{p-2} \nabla u$, as defined in Section 2.1.

Remark 3. The GMsFEM numerical solution u_{ms} in (4) is uniquely defined. We suppose there are two solutions $u_1 = H_p(\sum_i \sum_{k=1}^{L_i} \chi_i c_{k,1}^{\omega_i} \phi_k^{\omega_i})$ and $u_2 = H_p(\sum_i \sum_{k=1}^{L_i} \chi_i c_{k,2}^{\omega_i} \phi_k^{\omega_i})$ to (4). Then, we have

$$\int_D (a(x, \nabla u_1) - a(x, \nabla u_2)) \cdot \nabla v dx = 0,$$

for any test function. Since u_1 and u_2 are harmonic in each coarse block, we have

$$\int_D \kappa(x) |\nabla u_1 - \nabla u_2|^p dx \leq \int_D (a(x, \nabla u_1) - a(x, \nabla u_2)) \cdot \nabla (u_1 - u_2) dx = 0,$$

which guarantees $u_1 = u_2$. So the solution to (4) is uniquely defined.

3.1. **Partition of unity functions.** To propose our method, we first need to construct a set of partition of unity functions $\{\chi_i\}_{i=1}^{N_v}$. These functions are supported in coarse neighborhoods, and summed to one. Specifically, the support of χ_i is ω_i, and $\sum_{i=1}^{N_v} \chi_1 = 1$. In addition, χ_i has value 1 at the vertex y_i. There are two commonly used sets of partition of unity functions, which are presented below.

- A bilinear partition of unity: χ_i is defined as usual bilinear basis functions χ_i^0 on ω_i, which is equal to 1 at node y_i and equal to 0 on $\partial\omega_i$.
- A multiscale partition of unity (with linear boundary conditions): χ_i is defined by

$$-div(a(x, \nabla \chi_i) = 0 \text{ in } K \in \omega_i, \quad \chi_i = \chi_i^0 \text{ on } \partial K, \text{ for all } K \in \omega_i.$$

We remark that using the second choice of partition of unity functions can, in general, provide better numerical performance.

3.2. **Generalized multiscale finite element basis.**

3.2.1. *Snapshot space.* Let ω_i be a given coarse neighborhood. The construction of the multiscale basis functions on ω_i starts with a snapshot space $V_{\text{snap}}^{\omega_i}$. The snapshot space $V_{\text{snap}}^{\omega_i}$ is a set of functions defined on ω_i and contains all or most necessary components of the fine-scale solution restricted to ω_i. A spectral problem is then solved in the snapshot space to extract the dominant modes in the snapshot space. These dominant modes are the offline basis functions and the resulting reduced space is called the offline space. There are two choices of $V_{\text{snap}}^{\omega_i}$ that are commonly used.

The first choice is to use all possible fine-grid functions in ω_i. This snapshot space provides accurate approximation for the solution space; however, this snapshot space can be very large. The second choice for the snapshot space consists of harmonic extensions. In particular, we denote by $M_h(\omega_i)$ the set of all nodes of the fine mesh $\mathcal{T}^h$ which lie on $\partial\omega_i$. For each fine-grid node $x_j \in M_h(\omega_i)$, we construct a discrete delta function $\delta_j^h(x)$ defined on $M_h(\omega_i)$ by

$$\delta_j^h(x_k) = \begin{cases} 1 & \text{for } k = j \\ 0 & \text{for } k \neq j \end{cases}, \qquad \forall x_k \in M_h(\omega_i).$$

Then the $j-$th snapshot basis function $\psi_j^{\omega_i}$ is defined as the solution of

$$\begin{aligned} -div(\kappa(x)\nabla\psi_j^{\omega_i}) &= 0 \quad \text{in } \omega_i, \\ \psi_j^{\omega_i} &= \delta_j^h \text{ on } \partial\omega_i. \end{aligned} \tag{5}$$

The dimension of $V_{\text{snap}}^{\omega_i}$ is equal to the size of $M_h(\omega_i)$. We note that one can use randomized snapshots in conjunction with oversampling to reduce the computational cost associated with the snapshot calculations. We refer to [12] for more details.

With these snapshots, we follow the procedure in the following subsection to generate offline basis functions by using an auxiliary spectral decomposition.

3.2.2. *Offline space.* The construction of generalized multiscale basis for solving p-Laplacian equation in the fashion of p-harmonic extension is based on the design of a proper nonlinear spectral problem which will be solved in the snapshot space. In each coarse neighborhood ω_i, we define the following nonlinear eigenvalue problem which can be characterized by the Rayleigh-Ritz method (RRM).

$$\begin{cases} \phi_1^{\omega_i} = c^{\omega_i}, & \lambda_1^{\omega_i} = 0, \\ \phi_k^{\omega_i} = \arg\min\limits_{v \in V_{\text{snap}}^{\omega_i}} \dfrac{G^{\omega_i}(v)}{G_\chi^{\omega_i}(v - P_{k-1}(v))}, & \lambda_k^{\omega_i} = \dfrac{G^{\omega_i}(\phi_k^{\omega_i})}{G_\chi^{\omega_i}(\phi_k^{\omega_i} - P_{k-1}(\phi_k^{\omega_i}))}, \text{ for } k \geq 2, \end{cases} \tag{6}$$

where $c^{\omega_i} \in V_{\text{snap}}^{\omega_i}$ is a constant function in ω_i, the functionals are given by $G^{\omega_i}(v) = \int_{\omega_i} \kappa(x)|\nabla H_p(v)|^p dx$ and $G_\chi^{\omega_i}(v) = \int_{\omega_i} \kappa(x)|\nabla H_p(\chi_i v)|^p dx$, the projector $P_k(u) = \arg\min\limits_{v \in V_{k-1}^{\omega_i}} G^{\omega_i}(u - v)$, $V_{k-1}^{\omega_i} = \text{span}\{\phi_1^{\omega_i}, \cdots, \phi_{k-1}^{\omega_i}\}$. This nonlinear eigenvalue problem is a standard orthogonal subspace minimization method and is well-defined (see e.g., [50]).

The eigenfunctions $\{\phi_k^{\omega_i}\}_k$ in each coarse neighborhood ω_i will contribute as offline basis (or we call them generalized multiscale basis or eigenbasis) after being multiplied

by the associated partition of unity function χ_i. We choose the first L_i eigenfunctions on each ω_i and denote the offline space as

$$V^c = \text{span}\{\chi_i \phi_k^{\omega_i} : k = 1, \cdots, L_i;\ i = 1, \cdots, N_v\} \subseteq W^{1,p}(D).$$

Recall that our solution assumes the form of $u_{ms} = H_p(\sum_i \sum_{k=1}^{L_i} c_k^{\omega_i} \chi_i \phi_k^{\omega_i})$, which means u_{ms} is obtained by p-harmonically extending $\sum_i \sum_{k=1}^{L_i} c_k^{\omega_i} \chi_i \phi_k^{\omega_i}$ in each coarse block K, thus only the values of $\sum_i \sum_{k=1}^{L_i} c_k^{\omega_i} \chi_i \phi_k^{\omega_i}$ on each coarse edge matter in this sense. If we consider one coarse neighborhood ω_i, for example the coarse neighborhood of an interior coarse vertex (see y_i and ω_i in Figure 2), it is the restriction of $\sum_{k=1}^{L_i} c_k^{\omega_i} \chi_i \phi_k^{\omega_i}$ on the 12 coarse edges that will matter in the process of p-harmonic extension. Notice that the partition of unity function χ_i vanishes on and beyond the boundary of ω_i, thus merely the restriction of $\sum_{k=1}^{L_i} c_k^{\omega_i} \chi_i \phi_k^{\omega_i}$ on the *cross* (that is, the inside 4 coarse edges) makes an influence. Therefore, we can restrict $\chi_i \phi_k^{\omega_i}$ $(k = 1, \cdots, L_i)$ on the cross of ω_i and denote the restricted basis (which we call *cross basis* in this context) by $\hat{\phi}_k^{\omega_i}$. Then we can write $u_{ms} = H_p(\sum_i \sum_{k=1}^{L_i} c_k^{\omega_i} \hat{\phi}_k^{\omega_i})$. We denote

$$\widehat{V}^c = \text{span}\{\hat{\phi}_k^{\omega_i} : k = 1, \cdots, L_i;\ i = 1, \cdots, N_v\}.$$

In this way, we can focus on the degree of freedoms on the crosses and perform spectral decomposition on these crosses.

Remark 4. In the computation, we use a simpler eigenvalue problem

$$\begin{cases} \phi_1^{\omega_i} = c^{\omega_i}, & \lambda_1^{\omega_i} = 0, \\ \phi_k^{\omega_i} = \arg \min\limits_{v \in X_k^{\omega_i}} \dfrac{G^{\omega_i}(v)}{G_\chi^{\omega_i}(v)}, & \lambda_k^{\omega_i} = \dfrac{G^{\omega_i}(\phi_k^{\omega_i})}{G_\chi^{\omega_i}(\phi_k^{\omega_i})}, \quad \text{for} \quad k \geq 2, \end{cases} \tag{7}$$

where $X_k^{\omega_i}$ is a subspace of $V_{\text{snap}}^{\omega_i}$ and defined as $X_k^{\omega_i} = \left(\text{span}\{\phi_1^{\omega_i}, \cdots, \phi_{k-1}^{\omega_i}\}\right)^\perp$ where the orthogonality $\perp$ is defined with respect to the H^1 norm in $V_{\text{snap}}^{\omega_i}$.

4. **Convergence analysis.** To analyze the convergence of our proposed method, we first prove several lemmas. The first two lemmas are the direct applications of Lemmas 5.1 and 5.3 in Glowinski and Marrocco [35] and prove the monotonicity and continuity of p-Laplacian operator $a(x, \nabla u) = \kappa(x)|\nabla u|^{p-2}\nabla u$, respectively. In the following proof, we introduce the notation $F \preceq G$ to represent $F \leq \mathcal{C}G$ with a constant $\mathcal{C}$ independent of the mesh, contrast and the functions involved.

Lemma 4.1. *$\forall u, v \in W^{1,p}(K)$, $p \geq 2$, the following inequality holds:*

$$\kappa(x)|\nabla u - \nabla v|^p \preceq (a(x, \nabla u) - a(x, \nabla v)) \cdot \nabla(u - v). \tag{8}$$

Proof. We use Lemma 5.1 in Glowinski and Marrocco [35], which proves the following inequality: $\forall p \geq 2$, $\exists \alpha > 0$ such that $\forall y, z \in \mathbf{R}^2$,

$$(|z|^{p-2}z - |y|^{p-2}y, z - y)_{\mathbf{R}^2} \geq \alpha |z - y|^p.$$

If we take $z = (\kappa(x))^{1/p}\nabla u, y = (\kappa(x))^{1/p}\nabla v$, then (8) is proved. □

Lemma 4.2. *$\forall u, v \in W^{1,p}(K)$, $p \geq 2$, the following inequality holds:*

$$|a(x, \nabla u) - a(x, \nabla v))| \preceq M(x, u, v)|\nabla u - \nabla v|, \tag{9}$$

where $M(x, u, v) = \kappa(x)(|\nabla u| + |\nabla v|)^{p-2}$.

Proof. According to Lemma 5.3 in Glowinski and Marrocco [35], there holds the following inequality: $\forall p \geq 2$, $\exists \beta > 0$ such that $\forall y, z \in \mathbf{R}^2$,

$$||z|^{p-2}z - |y|^{p-2}y| \leq \beta |z-y|(|z|+|y|)^{p-2}.$$

If we take $z = (\kappa(x))^{1/(p-1)}\nabla u, y = (\kappa(x))^{1/(p-1)}\nabla v$, then (9) is proved. □

The next two lemmas deal with the properties of p-harmonic extension operator.

Lemma 4.3. *Suppose* $\tilde{u} = H_p(u_0), \tilde{v} = H_p(v_0), \tilde{w} = H_p(u_0 - v_0)$, *where* $u_0, v_0 \in W^{1,p}(K)$, $p \geq 2$. *Then we have*

$$\begin{aligned} &\int_K \kappa(x)|\nabla(\tilde{u}-\tilde{v})|^p dx \\ &\preceq \left(\int_K \kappa(x)|\nabla\tilde{w}|^p dx\right)^{\frac{q}{p}} \left(\int_K \kappa(x)|\nabla\tilde{u}|^p dx + \int_K \kappa(x)|\nabla\tilde{v}|^p dx\right)^{\frac{p-2}{p-1}}, \end{aligned} \tag{10}$$

where $1/p + 1/q = 1$.

Proof. Using Lemma 4.1 and integrating by parts, we immediately obtain the following inequality:

$$\begin{aligned} &\int_K \kappa(x)|\nabla(\tilde{u}-\tilde{v})|^p dx \preceq \int_K (a(x,\nabla\tilde{u}) - a(x,\nabla\tilde{v}))\cdot\nabla(\tilde{u}-\tilde{v}) \\ &= \int_{\partial K} (a(x,\nabla\tilde{u}) - a(x,\nabla\tilde{v}))\cdot\vec{n}(\tilde{u}-\tilde{v})ds - \int_K div(a(x,\nabla\tilde{u}) - a(x,\nabla\tilde{v}))\,(\tilde{u}-\tilde{v})dx \\ &= \int_{\partial K} (a(x,\nabla\tilde{u}) - a(x,\nabla\tilde{v}))\cdot\vec{n}\,(\tilde{u}-\tilde{v})ds - 0 \\ &= \int_{\partial K} (a(x,\nabla\tilde{u}) - a(x,\nabla\tilde{v}))\cdot\vec{n}\,\tilde{w}ds - \int_K div(a(x,\nabla\tilde{u}) - a(x,\nabla\tilde{v}))\,\tilde{w}dx \\ &= \int_{\partial K} (a(x,\nabla\tilde{u}) - a(x,\nabla\tilde{v}))\cdot\nabla\tilde{w}dx \\ &\preceq \int_K M(x,\tilde{u},\tilde{v})|\nabla\tilde{u}-\nabla\tilde{v}||\nabla\tilde{w}|dx, \end{aligned} \tag{11}$$

where on the last line we have used the continuity property of $a(x,\nabla u)$ proved in Lemma 4.2. Applying Hölder's inequality to (11), we have

$$\begin{aligned} \int_K \kappa(x)|\nabla(\tilde{u}-\tilde{v})|^p dx &\preceq \left(\int_K \kappa(x)|\nabla\tilde{u}-\nabla\tilde{v}|^p dx\right)^{\frac{1}{p}} \\ \left(\int_K \kappa(x)|\nabla\tilde{w}|^p dx\right)^{\frac{1}{p}} &\left(\int_K \left(\kappa(x)^{-\frac{2}{p}}\,|M(x,\tilde{u},\tilde{v})|\,\right)^{\frac{p}{p-2}} dx\right)^{\frac{p-2}{p}}. \end{aligned}$$

Dividing both sides by $\left(\int_K \kappa(x)|\nabla\tilde{u}-\nabla\tilde{v}|^p dx\right)^{\frac{1}{p}}$ gives

$$\int_K \kappa(x)|\nabla(\tilde{u}-\tilde{v})|^p dx \preceq \left(\int_K \kappa(x)|\nabla\tilde{w}|^p dx\right)^{\frac{q}{p}} \left(\int_K \left(\kappa(x)^{-\frac{2}{p}}\,|M(x,\tilde{u},\tilde{v})|\,\right)^{\frac{p}{p-2}} dx\right)^{\frac{p-2}{p-1}}. \tag{12}$$

Recall from Lemma 4.2 that $M(x,\tilde{u},\tilde{v}) = \kappa(x)(|\nabla\tilde{u}| + |\nabla\tilde{v}|)^{p-2}$, thus

$$\left(\int_K \left(\kappa(x)^{-\frac{2}{p}}\,|M(x,\tilde{u},\tilde{v})|\,\right)^{\frac{p}{p-2}} dx\right)^{\frac{p-2}{p-1}} = \left(\int_K \kappa(x)(|\nabla\tilde{u}| + |\nabla\tilde{v}|)^p dx\right)^{\frac{p-2}{p-1}}$$

$$\preceq \left(\int_K \kappa(x) |\nabla \tilde{u}|^p dx + \int_K \kappa(x) |\nabla \tilde{v}|^p dx \right)^{\frac{p-2}{p-1}}. \tag{13}$$

We substitute (13) into (12), and we then see that (10) is proved. □

Lemma 4.4. *For any $u_0, v_0 \in W^{1,p}(K)$, $p \geq 2$, we have*

$$\int_K \kappa(x) |\nabla H_p(u_0 + v_0)|^p dx \leq \int_K \kappa(x) |\nabla (H_p(u_0) + H_p(v_0))|^p dx. \tag{14}$$

Proof. Recall Remark 1, we have

$$\int_K \kappa(x) |\nabla H_p(u)|^p dx = \min_{v \in W_u^{1,p}(K)} \int_K \kappa(x) |\nabla v|^p dx.$$

Therefore,

$$\begin{aligned}
\int_K \kappa(x) |\nabla H_p(u_0 + v_0)|^p dx &= \min_{w \in W^{1,p}_{u_0+v_0}(K)} \int_K \kappa(x) |\nabla w|^p dx \\
&= \min_{w_1 + w_2 \in W^{1,p}_{u_0+v_0}(K)} \int_K \kappa(x) |\nabla (w_1 + w_2)|^p dx \\
&\leq \min_{w_1 \in W^{1,p}_{u_0}(K),\, w_2 \in W^{1,p}_{v_0}(K)} \int_K \kappa(x) |\nabla (w_1 + w_2)|^p dx.
\end{aligned}$$

Taking $w_1 = H_p(u_0), w_2 = H_p(v_0)$, we obtain

$$\int_K \kappa(x) |\nabla H_p(u_0 + v_0)|^p dx \leq \int_K \kappa(x) |\nabla (H_p(u_0) + H_p(v_0))|^p dx.$$

□

4.1. **Main convergence result.** We will show the main convergence result in this section. First, we will prove Lemma 4.5 which approximates the error of GMsFEM solution by using functions from the offline space V^c.

Lemma 4.5. *Suppose u is the exact solution of Equation (2), u_{ms} is the GMsFEM solution from Equation (4), then for any $p \geq 2$, we have*

$$\|u - u_{ms}\|_{1,p(D)} \preceq \|u - H_p(v_H)\|^{\frac{q}{p}}_{1,p(D)} \|u\|^{\frac{p-2}{p-1}}_{1,p(D)} \quad \text{for any } v_H \in V^c,$$

where $1/p + 1/q = 1$, $\|u\|_{1,p(D)} = \left(\int_D \kappa(x) |\nabla u|^p dx\right)^{1/p}$ is the energy norm defined in Section 2.1.

Proof. Using Lemma 4.1, we immediately obtain the following inequality:

$$\begin{aligned}
\int_D \kappa(x) |\nabla (u - u_{ms})|^p dx &\preceq \int_D (a(x, \nabla u) - a(x, \nabla u_{ms})) \cdot \nabla (u - u_{ms}) \\
&= \int_D (a(x, \nabla u) - a(x, \nabla u_{ms})) \cdot \nabla (u - H_p(v_H)) \\
&\preceq \int_D M(x, u, u_{ms}) |\nabla u - \nabla u_{ms}| |\nabla u - \nabla H_p(v_H)| dx,
\end{aligned}$$

for any $v_H \in V^c$, where on the last line we have used the continuity property of $a(x, \nabla u)$. Applying Hölder's inequality, we have

$$\int_D \kappa(x) |\nabla (u - u_{ms})|^p dx$$

$$\preceq \left(\int_D \kappa(x)|\nabla(u-u_{ms})|^p dx\right)^{\frac{1}{p}} \left(\int_D \kappa(x)|\nabla(u-H_p(v_H))|^p dx\right)^{\frac{1}{p}} \left(\int_D \left(\kappa(x)^{-\frac{2}{p}}\,|M(x,u,u_{ms})|\right)^{\frac{p}{p-2}} dx\right)^{\frac{p-2}{p}}.$$

Dividing both sides by $\left(\int_D \kappa(x)|\nabla(u-u_{ms})|^p dx\right)^{\frac{1}{p}}$ gives

$$\begin{aligned}
&\int_D \kappa(x)|\nabla(u-u_{ms})|^p dx \preceq \left(\int_D \kappa(x)|\nabla(u-H_p(v_H))|^p dx\right)^{\frac{q}{p}} \times \\
&\left(\int_D \left(\kappa(x)^{-\frac{2}{p}}\,|M(x,u,u_{ms})|\right)^{\frac{p}{p-2}} dx\right)^{\frac{p-2}{p-1}} \\
&= \left(\int_D \kappa(x)|\nabla(u-H_p(v_H))|^p dx\right)^{\frac{q}{p}} \times \\
&\left(\int_D \left(\kappa(x)^{-\frac{2}{p}}\cdot\kappa(x)(|\nabla u|+|\nabla u_{ms}|)^{p-2}\right)^{\frac{p}{p-2}} dx\right)^{\frac{p-2}{p-1}} \\
&= \left(\int_D \kappa(x)|\nabla(u-H_p(v_H))|^p dx\right)^{\frac{q}{p}} \left(\int_D \kappa(x)(|\nabla u|+|\nabla u_{ms}|)^p dx\right)^{\frac{p-2}{p-1}} \\
&\preceq \left(\int_D \kappa(x)|\nabla(u-H_p(v_H))|^p dx\right)^{\frac{q}{p}} \left(\int_D \kappa(x)(|\nabla u|^p+|\nabla u_{ms}|^p) dx\right)^{\frac{p-2}{p-1}} \\
&\preceq \left(\int_D \kappa(x)|\nabla(u-H_p(v_H))|^p dx\right)^{\frac{q}{p}} \left(\int_D \kappa(x)|\nabla u|^p dx + \int_D \kappa(x)|\nabla u_{ms}|^p dx\right)^{\frac{p-2}{p-1}} \\
&\preceq \left(\int_D \kappa(x)|\nabla(u-H_p(v_H))|^p dx\right)^{\frac{q}{p}} \left(\int_D \kappa(x)|\nabla u|^p dx\right)^{\frac{p-2}{p-1}}.
\end{aligned}$$

It follows immediately

$$\|u-u_{ms}\|_{1,p(D)} \preceq \|u-H_p(v_H)\|^{\frac{q}{p}}_{1,p(D)} \|u\|^{\frac{p-2}{p-1}}_{1,p(D)}.$$

□

Lemma 4.6. *Suppose u is the exact solution of Equation (2), K is any coarse block of size H, $p \geq 2$, then we have*

$$\int_K \kappa(x)|\nabla(u-H_p(u))|^p dx \preceq H^q \int_K |f|^q dx, \tag{15}$$

where $1/p + 1/q = 1$.

Proof. It's clear that

$$-div(a(x,\nabla u) - a(x,\nabla H_p(u))) = f.$$

Thus,

$$\int_K (a(x,\nabla u) - a(x,\nabla H_p(u)))\cdot\nabla(u-H_p(u)) dx = \int_K (u-H_p(u)) f dx.$$

By Lemma 4.1,

$$\int_K \kappa(x)|\nabla(u-H_p(u))|^p dx \preceq \int_K |u-H_p(u)||f| dx$$

$$\preceq \left(\int_K |u - H_p(u)|^p dx\right)^{\frac{1}{p}} \left(\int_K |f|^q dx\right)^{\frac{1}{q}}.$$

Using Poincaré's inequality, we get

$$\begin{aligned}\int_K \kappa(x)|\nabla(u - H_p(u))|^p dx &\preceq H \left(\int_K |\nabla(u - H_p(u))|^p dx\right)^{\frac{1}{p}} \left(\int_K |f|^q dx\right)^{\frac{1}{q}} \\ &= \kappa_0^{-\frac{1}{p}} H \left(\int_K \kappa_0 |\nabla(u - H_p(u))|^p dx\right)^{\frac{1}{p}} \left(\int_K |f|^q dx\right)^{\frac{1}{q}} \\ &\preceq H \left(\int_K \kappa(x)|\nabla(u - H_p(u))|^p dx\right)^{\frac{1}{p}} \left(\int_K |f|^q dx\right)^{\frac{1}{q}}.\end{aligned}$$

Dividing both sides by $\left(\int_K \kappa(x)|\nabla(u - H_p(u))|^p dx\right)^{\frac{1}{p}}$, we get

$$\int_K \kappa(x)|\nabla(u - H_p(u))|^p dx \preceq H^q \int_K |f|^q dx.$$

□

Remark 5. This local error estimate proved in Lemma 4.6 immediately deduces the global error estimate:

$$\|u - H_p(u)\|^p_{1,p(D)} \preceq H^q \|f\|^q_{L^q(D)}. \tag{16}$$

Now, we come to the main convergence theorem.

Theorem 4.7. *Suppose u is the exact solution of Equation (2), u_{ms} is the GMsFEM solution from Equation (4), then for any $p \geq 2$, we have*

$$\|u - u_{ms}\|_{1,p(D)} \preceq \|u\|^{\frac{p-2}{p-1}}_{1,p(D)} \left\{ H^{\frac{1}{(p-1)^2}} \|f\|^{\frac{1}{(p-1)^2}}_{L^q(D)} + \left(\frac{1}{\Lambda_*}\right)^{\frac{1}{p(p-1)^2}} \|u\|^{\frac{1}{p-1}}_{1,p(D)} \right\}, \tag{17}$$

where $\Lambda_* = \min_{\omega_i} \lambda^{\omega_i}_{L_i+1}$, $\{\lambda^{\omega_i}_j\}$ are the eigenvalues defined by (6) in Section 3.2.2, L_i is the number of eigenbasis chosen in each coarse neighborhood ω_i.

Proof. We first define the interpolation of u onto the offline space V^c as

$$I_0 u = \arg\min_{v \in V^c} \{\|u - H_p(v)\|_{1,p(D)}\}.$$

Since $I_0 u \in V^c$, we denote $I_0 u = \sum_i \chi_i u_0^{\omega_i}$, where $u_0^{\omega_i} = \sum_{k=1}^{L_i} c_k^{\omega_i} \phi_k^{\omega_i}$. By Lemma 4.5 and (16), it follows that

$$\begin{aligned}\|u - u_{ms}\|_{1,p(D)} &\preceq \|u\|^{\frac{p-2}{p-1}}_{1,p(D)} \|u - H_p(I_0 u)\|^{\frac{q}{p}}_{1,p(D)} \\ &\preceq \|u\|^{\frac{p-2}{p-1}}_{1,p(D)} \left(\|u - H_p(u)\|_{1,p(D)} + \|H_p(u) - H_p(I_0 u)\|_{1,p(D)}\right)^{\frac{q}{p}} \\ &\preceq \|u\|^{\frac{p-2}{p-1}}_{1,p(D)} \left(\|u - H_p(u)\|^{\frac{q}{p}}_{1,p(D)} + \|H_p(u) - H_p(I_0 u)\|^{\frac{q}{p}}_{1,p(D)}\right) \\ &\preceq \|u\|^{\frac{p-2}{p-1}}_{1,p(D)} \left(H^{\frac{q^2}{p^2}} \|f\|^{\frac{q^2}{p^2}}_{L^q(D)} + \|H_p(u) - H_p(I_0 u)\|^{\frac{q}{p}}_{1,p(D)}\right) \\ &= \|u\|^{\frac{p-2}{p-1}}_{1,p(D)} \left(H^{\frac{1}{(p-1)^2}} \|f\|^{\frac{1}{(p-1)^2}}_{L^q(D)} + \|H_p(u) - H_p(I_0 u)\|^{\frac{1}{p-1}}_{1,p(D)}\right). \end{aligned} \tag{18}$$

In the following, we will estimate $\|H_p(u) - H_p(I_0 u)\|^{\frac{1}{p-1}}_{1,p(D)}$.

Using Lemma 4.3, we have

$$\|H_p(u)-H_p(I_0u)\|^p_{1,p(D)} \preceq \left(\int_D \kappa(x)|\nabla H_p(u-I_0u)|^p dx\right)^{\frac{q}{p}} \times \tag{19}$$

$$\left(\int_D \kappa(x)|\nabla H_p(u)|^p dx + \int_D \kappa(x)|\nabla H_p(I_0u)|^p dx\right)^{\frac{p-2}{p-1}}$$

$$\preceq \left(\int_D \kappa(x)|\nabla H_p(\sum_{\omega_i}\chi_i(u-u_0^{\omega_i}))|^p dx\right)^{\frac{q}{p}} \left(\int_D \kappa(x)|\nabla u|^p dx\right)^{\frac{p-2}{p-1}}. \tag{20}$$

Applying the property of $H_p(\cdot)$ proved in Lemma 4.4 to (20), we achieve

$$\|H_p(u)-H_p(I_0u)\|^p_{1,p(D)} \preceq \left(\int_D \sum_{\omega_i}\kappa(x)|\nabla H_p(\chi_i(u-u_0^{\omega_i}))|^p dx\right)^{\frac{q}{p}} \times$$

$$\left(\int_D \kappa(x)|\nabla u|^p dx\right)^{\frac{p-2}{p-1}}$$

$$\preceq \left(\sum_{\omega_i}\int_{\omega_i} \kappa(x)|\nabla H_p(\chi_i(u-u_0^{\omega_i}))|^p dx\right)^{\frac{q}{p}} \left(\int_D \kappa(x)|\nabla u|^p dx\right)^{\frac{p-2}{p-1}}. \tag{21}$$

Recall that $u_0^{\omega_i} = \sum_{k=1}^{L_i} c_k^{\omega_i}\phi_k^{\omega_i}$ with $\{\phi_k^{\omega_i}\}$ being eigenfunctions defined by (6) in Section 3.2.2. We have the following inequality

$$\int_{\omega_i} \kappa(x)|\nabla H_p(\chi_i(u-u_0^{\omega_i}))|^p dx \preceq \frac{1}{\lambda_{L_i+1}}\int_{\omega_i}\kappa(x)|\nabla H_p(u-u_0^{\omega_i})|^p dx. \tag{22}$$

Define $\Lambda_* = \min_{\omega_i}\lambda_{L_i+1}^{\omega_i}$, then through (21) and (22) we get

$$\|H_p(u)-H_p(I_0u)\|^p_{1,p(D)} \preceq \left(\sum_{\omega_i}\frac{1}{\lambda_{L_i+1}}\int_{\omega_i}\kappa(x)|\nabla H_p(u-u_0^{\omega_i})|^p dx\right)^{\frac{q}{p}} \times \tag{23}$$

$$\left(\int_D \kappa(x)|\nabla u|^p dx\right)^{\frac{p-2}{p-1}}$$

$$\preceq \left(\frac{1}{\Lambda_*}\sum_{\omega_i}\int_{\omega_i}\kappa(x)|\nabla H_p(u-u_0^{\omega_i})|^p dx\right)^{\frac{q}{p}} \left(\int_D \kappa(x)|\nabla u|^p dx\right)^{\frac{p-2}{p-1}}$$

$$= \left(\frac{1}{\Lambda_*}\right)^{\frac{q}{p}} \left(\sum_{\omega_i}\int_{\omega_i}\kappa(x)|\nabla H_p(u-u_0^{\omega_i})|^p dx\right)^{\frac{q}{p}} \left(\int_D \kappa(x)|\nabla u|^p dx\right)^{\frac{p-2}{p-1}}$$

$$\preceq \left(\frac{1}{\Lambda_*}\right)^{\frac{q}{p}} \left(\int_D \kappa(x)|\nabla H_p(u)|^p dx\right)^{\frac{q}{p}} \left(\int_D \kappa(x)|\nabla u|^p dx\right)^{\frac{p-2}{p-1}}. \tag{24}$$

Using the energy minimization property of $H_p(\cdot)$ claimed in Remark 1, we obtain from (24) that

$$\|H_p(u)-H_p(I_0u)\|^p_{1,p(D)} \preceq \left(\frac{1}{\Lambda_*}\right)^{\frac{q}{p}} \left(\int_D \kappa(x)|\nabla u|^p dx\right)^{\frac{q}{p}} \left(\int_D \kappa(x)|\nabla u|^p dx\right)^{\frac{p-2}{p-1}}$$

$$= \left(\frac{1}{\Lambda_*}\right)^{\frac{q}{p}} \left(\int_D \kappa(x)|\nabla u|^p dx\right)^{\frac{q}{p}+\frac{p-2}{p-1}}$$

$$= \left(\frac{1}{\Lambda_*}\right)^{\frac{1}{p-1}} \int_D \kappa(x)|\nabla u|^p dx.$$

This gives

$$\|H_p(u) - H_p(I_0 u)\|_{1,p(D)}^{\frac{1}{p-1}} \preceq \left(\frac{1}{\Lambda_*}\right)^{\frac{1}{p(p-1)^2}} \|u\|_{1,p(D)}^{\frac{1}{p-1}}. \tag{25}$$

Substituting (25) into (18), we obtain

$$\|u - u_{ms}\|_{1,p(D)} \preceq \|u\|_{1,p(D)}^{\frac{p-2}{p-1}} \left\{ H^{\frac{1}{(p-1)^2}} \|f\|_{L^q(D)}^{\frac{1}{(p-1)^2}} + \left(\frac{1}{\Lambda_*}\right)^{\frac{1}{p(p-1)^2}} \|u\|_{1,p(D)}^{\frac{1}{p-1}} \right\}.$$

□

Remark 6. We notice that Λ^* will increase to infinity. Considering a function u with highly oscillating boundary conditions, the value of $\frac{G^{\omega_i}(u)}{G_\chi^{\omega_i}(u)}$ will be very large. More specifically, for u having highly oscillating boundary conditions, the value of $G^{\omega_i}(u)$ is large. But $\chi_i u$ will have less oscillation on the cross since u solves the harmonic problem. Therefore, $G_\chi^{\omega_i}(u)$ will be small and the ratio of $G^{\omega_i}(u)$ over $G_\chi^{\omega_i}(u)$ will be large.

Besides, we can improve the offline convergence rate by using multiple oversampled spectral problems. To be simple, we start with two eigenvalue problems. We denote $I_0^{\omega_i}(u) = u_0^{\omega_i}$, $\widetilde{\chi_i} = \frac{\chi_i}{\chi_i^+}$, $\tilde{u} = \chi_i^+(u - I_0^{\omega_i}(u))$, where χ_i^+ is the partition of unity function on the oversampled domain ω_i^+. Following inequality (21),

$$\begin{aligned}
\sum_{\omega_i} \int_{\omega_i} \kappa(x)|\nabla H_p(\chi_i(u - I_0^{\omega_i}(u)))|^p dx &= \sum_{\omega_i} \int_{\omega_i} \kappa(x)|\nabla H_p(\widetilde{\chi_i}(\tilde{u} - I_0^{\omega_i}(\tilde{u})))|^p dx \\
&\preceq \sum_{\omega_i} \frac{1}{\lambda_{L_i+1}^{\omega_i}} \int_{\omega_i} \kappa(x)|\nabla H_p(\tilde{u} - I_0^{\omega_i}(\tilde{u}))|^p dx \\
&\preceq \frac{1}{\Lambda_*} \sum_{\omega_i^+} \int_{\omega_i^+} \kappa(x)|\nabla H_p(\chi_i^+(u - I_0^{\omega_i}(u)))|^p dx \\
&\preceq \frac{1}{\Lambda_*} \sum_{\omega_i^+} \frac{1}{\lambda_{L_i+1}^{\omega_i^+}} \int_{\omega_i^+} \kappa(x)|\nabla H_p(u - I_0^{\omega_i}(u))|^p dx \\
&\preceq \frac{1}{\Lambda_*}\frac{1}{\Lambda_*^+} \sum_{\omega_i^+} \int_{\omega_i^+} \kappa(x)|\nabla H_p(u - I_0^{\omega_i}(u))|^p dx \\
&\preceq \frac{1}{\Lambda_*}\frac{1}{\Lambda_*^+} \int_D \kappa(x)|\nabla H_p(u)|^p dx \\
&\preceq \frac{1}{\Lambda_*}\frac{1}{\Lambda_*^+} \int_D \kappa(x)|\nabla u|^p dx,
\end{aligned}$$

where $\Lambda_* = \min_{\omega_i} \lambda_{L_i+1}^{\omega_i}$ and $\Lambda_*^+ = \min_{\omega_i^+} \lambda_{L_i+1}^{\omega_i^+}$. This result can be easily extended to multiple oversampled eigenvalue problems (instead of two eigenvalue problems), and the result would be

$$\sum_{\omega_i} \int_{\omega_i} \kappa(x)|\nabla H_p(\chi_i(u - I_0^{\omega_i}(u)))|^p dx \preceq \frac{1}{\Lambda_*}\frac{1}{\Lambda_*^+} \cdots \frac{1}{\Lambda_*^{+N}} \int_D \kappa(x)|\nabla u|^p dx,$$

where $\Lambda_*^{+N} = \min_{\omega_i^+} \lambda_{L_i+1}^{\omega_i^{+N}}$, ω_i^{+N} is a N layers oversampled domain (ω_i^+ is a 1 layer oversampled domain). We note that if we choose all these $\frac{1}{\Lambda_*}$ and $\frac{1}{\Lambda_*^{+k}}$'s to be less than some δ $(0 < \delta < 1)$, then $\frac{1}{\Lambda_*}\frac{1}{\Lambda_*^+}\cdots\frac{1}{\Lambda_*^{+N}} < \delta^{N+1}$ and the offline error would be exponential decay as the number of oversampled layers increases.

5. **Numerical implementation and results.** In this part, we exhibit the process of numerically implementing the proposed method for p-Laplacian equation. From Glowinski and Marrocco [35], or Ciarlet [19], $(\mathcal{P})$ is equivalent to the following minimization problem: $(\mathcal{Q})$ Find $u \in W_g^{1,p}(D) \equiv \{v \in W^{1,p}(D) : v = g \text{ on } \partial D\}$ such that

$$J_D(u) = \inf_{v \in W_g^{1,p}(D)} J_D(v), \tag{26}$$

where $J_D(u) = \frac{1}{p}\int_D \kappa(x)|\nabla u|^p dx - \int_D f u dx$.

It is easily established that $J_D(u)$ is strictly convex and continuous on $W_g^{1,p}(D)$. Besides, $J_D(u)$ is Gateaux differentiable with

$$J_D'(u)(w) = \int_D \kappa(x)|\nabla u|^{p-2}\nabla u \cdot \nabla w dx - \int_D f w dx \quad \forall w \in W_0^{1,p}(D).$$

Hence, there exists a unique solution to $(\mathcal{Q})$, and $(\mathcal{Q})$ is equivalent to its Euler equation $(\mathcal{P})$. The corresponding discrete problem of $(\mathcal{Q})$ is: $(\mathcal{Q}^h)$ Find $u^h \in V^h(D)$ such that

$$J_D(u^h) = \min_{v^h \in V_0^h(D)} J_D(v^h). \tag{27}$$

The well-posedness of $(\mathcal{Q}^h) = (\mathcal{P}^h)$ follows in an analogous way to that of $(\mathcal{Q})$ and $(\mathcal{P})$, see Glowinski and Marrocco [35] or Ciarlet [19].

Recall the discussion in Section 3.2.2, we can represent the GMsFEM solution by $u^h = H_p(\sum_i \sum_{k=1}^{L_i} c_k^{\omega_i}\hat{\phi}_k^{\omega_i})$. For notational brevity we use a single-index notation to write $u^h = H_p(\sum_{j=1}^N c_j\hat{\phi}_j)$. Then we apply *Broyden's method* (which is a Quasi-Newton's method) to solve the minimization problem $(\mathcal{Q}^h)$, see Algorithm 1.

Algorithm 1 A Quasi-Newton algorithm

Initialization: An initial guess $\vec{c}^{(0)} = \left(c_j^{(0)}\right)_{j=1}^N$ and $B^{(0)} \in \mathbb{R}^{N\times N}$

(1) Compute the gradient vector $\vec{g}^{(0)}(\vec{c}^{(0)}) = \nabla J_D(H_p(\sum_{j=1}^N c_j^{(0)}\hat{\phi}_j))$.

(2) Compute the stepsize $\tau^{(0)}$.

(3) Set: $\vec{c}^{(1)} = \vec{c}^{(0)} - \tau^{(0)}B^{(0)}\vec{g}^{(0)}$.

(4) **If** $\|\vec{c}^{(1)} - \vec{c}^{(0)}\| < \delta$, where $\|\cdot\|$ is a suitable norm, **return**.

for $k = 1$ to N: **do**

(1) Compute the gradient vector $\vec{g}^{(k)}(\vec{c}^{(k)}) = \nabla J_D(H_p(\sum_{j=1}^N c_j^{(k)}\hat{\phi}_j))$.

(2) Compute the approximation of the inverse of Hessian matrix:

$$B^{(k)} = B^{(k-1)} + \frac{[(\vec{c}^{(k)} - \vec{c}^{(k-1)}) - B^{(k-1)}(\vec{g}^{(k)} - \vec{g}^{(k-1)})](\vec{c}^{(k)} - \vec{c}^{(k-1)})^T B^{(k-1)}}{(\vec{c}^{(k)} - \vec{c}^{(k-1)})^T B^{(k-1)}(\vec{g}^{(k)} - \vec{g}^{(k-1)})}.$$

(3) Compute the stepsize $\tau^{(k)}$.

(4) Set: $\vec{c}^{(k+1)} = \vec{c}^{(k)} - \tau^{(k)}B^{(k)}\vec{g}^{(k)}$.

(5) **If** $\|\vec{c}^{(k+1)} - \vec{c}^{(k)}\| < \delta$, **return**.

end for

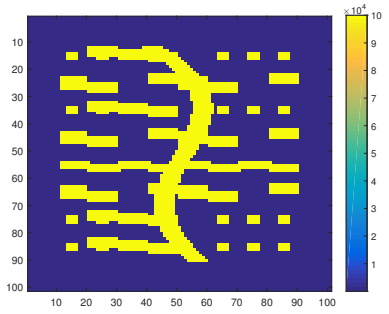

FIGURE 3. Illustration of the high-contrast permeability field $\kappa_1(x)$.

5.1. **Numerical results.** In this section, we offer a number of representative numerical results to verify the proposed methods in the previous sections. In particular, we solve Equation (2) using the proposed GMsFEM to validate the effectiveness of the respective approaches. To obtain benchmark fine-grid solutions we solve (2) on the unit square $D = [0,1] \times [0,1]$ using a uniform fine grid of 100×100 square finite elements which is divided into 10×10 square coarse elements uniformly. We also use a forcing term $f = 1$ and impose a linear Dirichlet boundary condition $u(x,y) = x + y$. The high-contrast permeability field $\kappa_1(x)$ used in our experiments is shown in Figure 3, with high-contrast ratio $\kappa_{\max}/\kappa_{\min}$ being 10^5. We note that the fine-grid discretization leads to a system of size $N_f = 10201$. As such, we aim to construct a reduced-order system that can accurately approximate the benchmark solutions from the original fine-scale system.

5.1.1. *Accuracy of GMsFEM using different numbers of basis functions.* We employ both fine-grid (FEM) and coarse-grid (GMsFEM) methods to solve the model equation (2). In comparing the respective approaches, we introduce relative L_p errors and relative energy errors, which are defined as

$$\begin{aligned} L_p \text{ error} &= \frac{\|u - u_{ms}\|_{L^p(D)}}{\|u\|_{L^p(D)}} \times 100\%, \\ \text{Energy error} &= \frac{\|u - u_{ms}\|_{1,p(D)}}{\|u\|_{1,p(D)}} \times 100\%, \end{aligned} \tag{28}$$

where we recall that u denotes the FEM solution and u_{ms} denotes the GMsFEM solution.

For the first set of experiments, we take $p = 3, 4, 5, 6$ separately and use different numbers of cross basis (L_i for each ω_i) for each fixed value of p. Then we check the relative errors of the GMsFEM solutions. Numerical results are shown in Table 1 and Figure 4. Note that in the first column of each sub-table, we show the numbers of basis functions used for each coarse neighborhood ω_i, and the degrees of freedom (DOF) of offline space which are the numbers in parentheses. To visually observe the accuracy of GMsFEM, we plot the solutions obtained by both FEM and GMsFEM in the case $p = 3$ using 4 cross basis functions in each coarse neighborhood, see Figure 5.

By observing the columns in Table 1 (or the curves in Figure 4), we can clearly see that for each p, the relative error decays as we use more cross basis functions. We note that as L_i increases, the the value of $(L_i + 1)$'s eigenvalue increases, and the error

bound $1/\Lambda_*$ will correspondingly decrease. In other words, the analysis suggests (and the results validate) that keeping more basis functions for the coarse space construction will indeed yield a decreasing global error. Through a more careful examination, we notice that for each p, when 4 or more than 4 cross basis are chosen in each coarse neighborhood (i.e. $L_i \geq 4$ for each ω_i), the errors are much smaller. This might suggest that if we use 4 or more than 4 cross basis in each coarse neighborhood, we would get a better convergence. We will explore this in more details in the following subsection.

L_i (DOF)	$p = 3$	
	L_p error	Energy error
1(81)	9.52 %	41.03 %
2(162)	6.45 %	34.38 %
3(243)	5.76 %	27.76 %
4(324)	0.52 %	6.55 %
5(405)	0.45 %	5.15 %
L_i (DOF)	$p = 4$	
	L_p error	Energy error
1(81)	10.88 %	42.35 %
2(162)	6.47 %	32.93 %
3(243)	5.12 %	24.13 %
4(324)	0.92 %	8.57 %
5(405)	0.82 %	6.65 %
L_i (DOF)	$p = 5$	
	L_p error	Energy error
1(81)	10.12 %	40.46 %
2(162)	7.71 %	34.05 %
3(243)	5.17 %	27.88 %
4(324)	0.94 %	9.94 %
5(405)	0.81 %	7.92 %
L_i (DOF)	$p = 6$	
	L_p error	Energy error
1(81)	8.95 %	39.68 %
2(162)	6.94 %	30.92 %
3(243)	4.37 %	23.85 %
4(324)	1.07 %	8.70 %
5(405)	0.91 %	7.08 %

TABLE 1. Relative errors for $p = 3, 4, 5, 6$ using different numbers of cross basis.

5.1.2. *Correlation between errors and eigenvalues.* Aside from the accuracy of our proposed method, we are interested in determining how many cross basis (or DOFs) should be used. As we mentioned earlier, there is a "jump" in the relative energy errors when we take 4 cross basis in each coarse neighborhood (i.e. $L_i = 4$ for each ω_i, see Table 1). Thus, $L_i = 4$ might be a good choice. According to our analysis in Section 4, that is probably due to a sudden decrease in the quantity of $1/\Lambda_*$, where $\Lambda_* = \min_{\omega_i} \lambda^{\omega_i}_{L_i+1}$, $\{\lambda^{\omega_i}_j\}$ are the eigenvalues defined in (7) in Section 3.2.2. To verify this theory, we calculate the corresponding $1/\Lambda_*$ for each L_i in the case of $p = 3$. The results are shown in Table 2. In this table, we see the jump in Λ_* and $1/\Lambda_*$ at $L_i = 4$, which

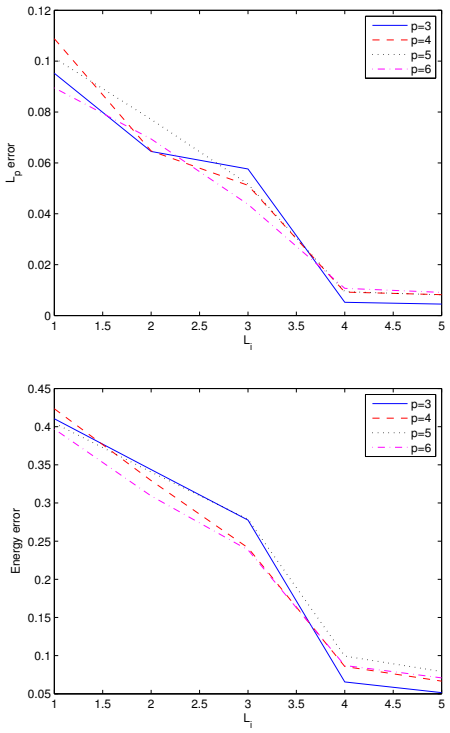

FIGURE 4. Relative error vs L_i for p=3,4,5,6.

explains our earlier inference. Hence, we conclude that the proper number of cross basis is chosen at the spot where there is a sudden increase in the values of Λ_* (or a sudden decrease in the values of $1/\Lambda_*$). We would like to remark that an adaptive method can be employed to determine a best choice of L_i for each coarse neighborhood ω_i. Moreover, to see a more quantitative relationship between the relative errors and the values of Λ_* as well as being inspired by the result in Theorem 4.7, we calculate the cross-correlation coefficient between the relative energy errors and the corresponding values of $(\frac{1}{\Lambda_*})^{\frac{1}{p(p-1)^2}}$ for the case $p = 3$. We recall that the quantity $(\frac{1}{\Lambda_*})^{\frac{1}{p(p-1)^2}}$ comes from (17) in Theorem 4.7. The evaluated cross-correlation coefficient is 0.99. This indicates a linear relationship between the relative energy error and the corresponding $(\frac{1}{\Lambda_*})^{\frac{1}{p(p-1)^2}}$, which verifies our result in (17).

L_i	Λ_*	$1/\Lambda_*$
1	8.86e-4	1.13e3
2	2.59e-3	3.86e2
3	4.46e-3	2.24e2
4	1.55e2	6.44e-3
5	4.01e2	2.50e-3

TABLE 2. Values of Λ_* and $1/\Lambda_*$ when $p = 3$.

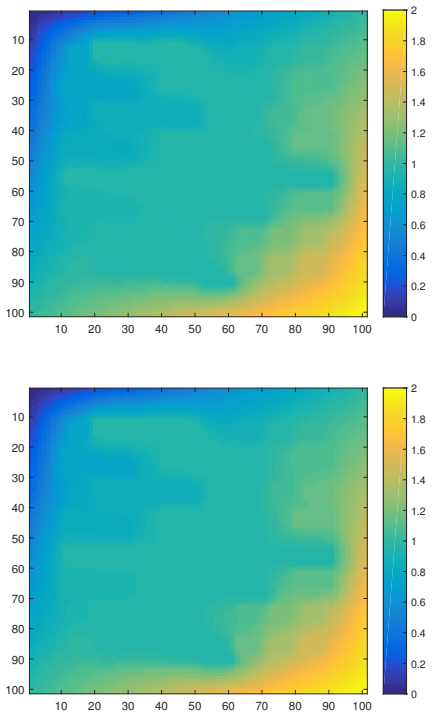

FIGURE 5. FEM v.s. GMsFEM node-wise solutions, p=3, DOF=324.

Remark 7. We note that the choice of L_i is highly related to the number of "channels" and "inclusions" in each coarse neighborhood. In more details, if there are m inclusions and channels in a coarse neighborhood ω_i , then one can observe m small, asymptotically vanishing, eigenvalues. In the example presented in this section, we can see that there are at most 4 inclusions and channels in each coarse neighborhood. This suggests the choice of $L_i = 4$, and we verify this choice by observing the values of Λ_i^*.

Since L_i is the number of eigen-pairs solved from the nonlinear eigenvalue problem, it's a finite number and can not grow to infinity. We can only guarantee that as L_i grows (not necessary to be a large number), the error will decay, which is observed by our numerical results.

5.1.3. *Numerical tests with more permeability fields.* To verify that our proposed method is applicable to more situations, we examine other choices of permeability field $\kappa(x)$. First, we would like to check that the GMsFEM solution errors do not depend on the high-contrast ratio $\kappa_{\max}/\kappa_{\min}$. To see this, we increase the high-contrast ratio of $\kappa_1(x)$, which is used in the previous subsections, from 10^5 to 10^7. We denote the new permeability field by $\kappa_2(x)$. Then we solve Equation (2) using both FEM and proposed GMsFEM, and calculate the relative errors and the error bound quantity $1/\Lambda_*$. Numerical results for $p = 3$ are shown in Table 3. Comparing these results with the top left sub-table in Table 1 and Table 2, we can observe similar trend inside the columns as well as a slight increase in the values of both relative energy errors and $1/\Lambda_*$'s. The jump at $L_i = 4$ still occurs. The cross-correlation coefficient between the relative energy errors and $(\frac{1}{\Lambda_*})^{\frac{1}{p(p-1)^2}}$ is calculated to be 0.98.

L_i	Energy error	$1/\Lambda_*$
1	44.15 %	1.42e3
2	36.44 %	4.04e2
3	27.99 %	2.35e2
4	6.77 %	6.49e-3
5	5.30 %	2.50e-3

TABLE 3. Relative energy errors and values of $1/\Lambda_*$ using $\kappa_2(x)$, $p = 3$.

We also consider a different high-contrast permeability field $\kappa_3(x)$, see Figure 6. We solve Equation (2) for $p = 3$ and the results are presented in Table 4. The cross-correlation coefficient between the relative energy errors and $(\frac{1}{\Lambda_*})^{\frac{1}{p(p-1)^2}}$ is calculated to be 0.94. Similar conclusions as made in Section 5.1.1 and 5.1.2 can be drawn for this new choice of permeability field. We can see that our proposed method works well for this permeability field.

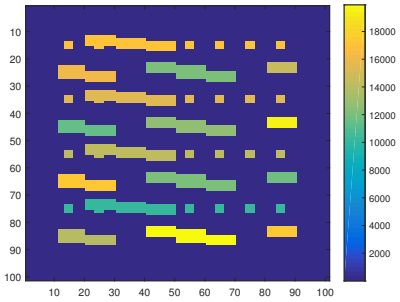

FIGURE 6. Illustration of the high-contrast permeability field $\kappa_3(x)$.

L_i	Energy error	$1/\Lambda_*$
1	47.08 %	1.85e1
2	27.68 %	4.64e0
3	20.81 %	2.68e0
4	4.33 %	2.26e-3
5	2.69 %	1.01e-3

TABLE 4. Relative energy errors and values of $1/\Lambda_*$ using $\kappa_3(x)$, $p = 3$.

5.1.4. *Comments on the computational cost.* The online cost is independent of fine mesh parameters, while it will grow as the spectral basis parameters increase. We note that the online cost is proportional to that of solving homogeneous p-Laplacian equation with polynomial basis. In practise, we usually only use a few spectral basis, so the online cost is close to that of solving homogeneous p-Laplacian equation with low order polynomial basis. We note that solving the nonlinear eigenvalue problem in each coarse neighborhood is one source of the computational cost. However, this is an offline step, which means when dealing with different forcing terms and boundary conditions

we only need to solve this nonlinear eigenvalue problem for a single time. Thus, the computation of this eigenvalue problem will not affect the online cost of our method. We also note that in Algorithm 1, a nonlinear function of the form $N(\nabla u) = \kappa(x)|\nabla u|^{p-2}$ requires a fine-grid update at each iterative step. In particular, at each iterative step, we must use the fine-scale solution values to construct a gradient and its norm, and we must subsequently multiply the resulting expressions with the original coefficient $\kappa(x)$ at all fine grid points in order to update the nonlinear permeability coefficient. This is a fine-grid dependent process that adds an increasing computational cost depending on the size of the fine grid. To decrease this cost, we introduce the discrete empirical interpolation method (DEIM), which allows us to approximate the nonlinear function on the fine grid while only evaluating at a few carefully selected points. In itself, DEIM is a snapshot-based preprocessing procedure in which the dominant spectral behavior of the global nonlinear function is extracted. We refer to [5] [48] for more detailed discussions on the use of DEIM. Moreover, by comparing the degrees of freedoms listed in Table 1 with the size of the fine-scale finite element system $N_f = 10201$, we see that we obtain a reduced sized system by applying generalized multiscale finite element method, which will reduce the computational cost.

Remark 8. Compared with the online cost, the offline cost depends on the fine mesh parameter, considering that each local snapshot problem is solved on the local coarse neighborhood consisting of fine grids. We note that the cost of numerical homogenization is high because the local problem $-div(a(x, \nabla N_{\xi_i})) = 0 \quad \text{in } K$ with boundary condition $N_{\xi_i} = \xi_i \cdot x$ on ∂K (K is a coarse block) is solved for all $\xi_1, \xi_2, \cdots, \xi_N$. Similarly, the local problem in offline stage is solved for all possible boundary conditions, which is consistent to numerical homogenization. So the offline cost is high. However, as mentioned in Section 3.2.1, one can use randomized snapshots in conjunction with oversampling to reduce the offline computational cost associated with the snapshot calculations. Also, one can select and compute eigenbasis adaptively in each coarse neighborhood which can eliminate the use of non-dominated modes and reduce offline cost. Besides, as mentioned above, DEIM is introduced to reduce offline computational cost when it comes to the evaluation of nonlinear functions.

Remark 9. To illustrate how the error of DEIM affects the global error estimate of Theorem 4.8, we adopt the notation $a_{DEIM}(x, \nabla u) = N_1(\nabla u)\nabla u$, where $N_1(\nabla u)(\approx \kappa(x)|\nabla u|^{p-2})$ is evaluated using DEIM. We denote $\tilde{u}_{ms}$ the DEIM solution which is obtained by solving

$$\int_D a_{DEIM}(x, \nabla \tilde{u}_{ms}) \cdot \nabla v = \int_D fv, \qquad \forall v \in V_0^h(D).$$

Then we have

$$\begin{aligned}
\|u_{ms} - \tilde{u}_{ms}\|^p_{1,p(D)} &= \int_D a(x, \nabla(u_{ms} - \tilde{u}_{ms})) \cdot \nabla(u_{ms} - \tilde{u}_{ms}) \\
&\leq \int_D a(x, \nabla u_{ms}) \cdot \nabla(u_{ms} - \tilde{u}_{ms}) - \int_D a(x, \nabla \tilde{u}_{ms}) \cdot \nabla(u_{ms} - \tilde{u}_{ms}) \\
&= \int_D (u_{ms} - \tilde{u}_{ms}) f - \int_D a(x, \nabla \tilde{u}_{ms}) \cdot \nabla(u_{ms} - \tilde{u}_{ms}) \\
&= \int_D (a_{DEIM}(x, \nabla \tilde{u}_{ms}) - a(x, \nabla \tilde{u}_{ms})) \cdot \nabla(u_{ms} - \tilde{u}_{ms}).
\end{aligned}$$

We note that $\|a_{DEIM}(x,\nabla\tilde{u}_{ms}) - a(x,\nabla\tilde{u}_{ms})\|$ is the DEIM error, which can be assumed to be a small quantity (ref. [5]). Then from the above inequality, it follows

$$\|u_{ms} - \tilde{u}_{ms}\|^p_{1,p(D)} \leq \delta^{p-1}\|u_{ms} - \tilde{u}_{ms}\|_{1,p(D)}, \tag{29}$$

for some small $\delta(0 < \delta < 1)$.

Combining (29) with Theorem 4.8, we obtain

$$\begin{aligned}\|u - \tilde{u}_{ms}\|_{1,p(D)} &\leq \|u - u_{ms}\|_{1,p(D)} + \|u_{ms} - \tilde{u}_{ms}\|_{1,p(D)} \\ &\preceq \delta + \|u\|^{\frac{p-2}{p-1}}_{1,p(D)} \left\{ H^{\frac{1}{(p-1)^2}} \|f\|^{\frac{1}{(p-1)^2}}_{L^q(D)} + \left(\frac{1}{\Lambda_*}\right)^{\frac{1}{p(p-1)^2}} \|u\|^{\frac{1}{p-1}}_{1,p(D)} \right\}.\end{aligned}$$

6. **Conclusion.** In this paper, our objective is to develop a multiscale model reduction using the framework of GMsFEM. We re-cast the problem and use the degrees of freedom defined on the boundaries of coarse elements (cf. hybridization techniques [20, 32, 15]). Our motivation stems from homogenization and the analysis of multiscale methods. Homogenization and numerical homogenization methods rely on nonlinear harmonic extensions of boundary values in order to capture the effects of scales within the domain. Via these local solutions, we can capture the effects of small separable scales. In the linear case, one can use a single basis per coarse element to capture these effects; however, for nonlinear problems, this is not possible because of non-additivity. Moreover, the use of degrees of freedom on the boundaries of coarse elements is important for achieving low dimensional approximate models. If nonlinear harmonic extensions are not used, one can not estimate the residuals (see [31]). In our framework, we propose a local nonlinear spectral decomposition, which select dominant modes in these nonlinear snapshot spaces. We present a convergence analysis and numerical results.

Acknowledgments. The authors would like to thank Wing Tat Leung for a number of insightful discussions regarding this work. YE would like to thank the partial support from NSF 1620318, the U.S. Department of Energy Office of Science, Office of Advanced Scientific Computing Research, Applied Mathematics program under Award Number DE-FG02-13ER26165 and National Priorities Research Program grant NPRP grant 7-1482-1278 from the Qatar National Research Fund.

REFERENCES

[1] A. Abdulle and G. Vilmart, Analysis of the finite element heterogeneous multiscale method for quasilinear elliptic homogenization problems, *Mathematics of Computation*, **83** (2014), 513–536.
[2] G. Allaire and R. Brizzi, A multiscale finite element method for numerical homogenization, *SIAM J. Multiscale Modeling and Simulation*, **4** (2005), 790–812.
[3] G. Allaire, Homogenization and two-scale convergence, *SIAM Journal on Mathematical Analysis*, **23** (1992), 1482–1518.
[4] T. Arbogast, Analysis of a two-scale, locally conservative subgrid upscaling for elliptic problems, *SIAM J. Numer. Anal.*, **42** (2004), 576–598 (electronic).
[5] M. Barrault, Y. Maday, N. C. Nguyen and A. T. Patera, An "empirical interpolation" method: Application to efficient reduced-basis discretization of partial differential equations, *Comptes Rendus Mathematique*, **339** (2004), 667–672.
[6] Y. Bazilevs, V. M. Calo, J. A. Cottrell, T. J. R. Hughes, A. Reali and G. Scovazzi, Variational multiscale residual-based turbulence modeling for large eddy simulation of incompressible flows, *Computer Methods in Applied Mechanics and Engineering*, **197** (2007), 173–201.
[7] L. Berlyand, Y. Gorb and A. Novikov, Discrete network approximation for highly-packed composites with irregular geometry in three dimensions, In *Multiscale Methods in Science and Engineering*, Springer, **44** (2005), 21–57.

[8] L. Berlyand, A. G. Kolpakov and A. Novikov, *Introduction to the Network Approximation Method for Materials Modeling*, Number 148. Cambridge University Press, 2013.
[9] L. Berlyand and A. Novikov, Error of the network approximation for densely packed composites with irregular geometry, *SIAM Journal on Mathematical Analysis*, **34** (2002), 385–408.
[10] L. Berlyand and H. Owhadi, Flux norm approach to finite dimensional homogenization approximations with non-separated scales and high contrast, *Archive for Rational Mechanics and Analysis*, **198** (2010), 677–721.
[11] V. M. Calo, Y. Efendiev, J. Galvis and M. Ghommem, Multiscale empirical interpolation for solving nonlinear PDEs, *Journal of Computational Physics*, **278** (2014), 204–220.
[12] V. M. Calo, Y. Efendiev, J. Galvis and G. Li, Randomized oversampling for generalized multiscale finite element methods, *Multiscale Model. Simul.,* **14** (2016), 482–501, http://arxiv.org/pdf/1409.7114.pdf.
[13] V. ChiadòPiat and A. Defranceschi, Homogenization of monotone operators, *Nonlinear Analysis: Theory, Methods & Applications*, **14** (1990), 717–732.
[14] C.-C. Chu, I. G. Graham and T.-Y. Hou, A new multiscale finite element method for high-contrast elliptic interface problems, *Math. Comp.*, **79** (2010), 1915–1955.
[15] E. Chung, B. Cockburn and G. Fu, The staggered dg method is the limit of a hybridizable dg method, *SIAM Journal on Numerical Analysis*, **52** (2014), 915–932.
[16] E. T. Chung, Y. Efendiev and W. T. Leung, An adaptive generalized multiscale discontinuous galerkin method (GMsDGM) for high-contrast flow problems, arXiv preprint, arXiv:1409.3474, 2014.
[17] E. T. Chung, Y. Efendiev and W. T. Leung, Residual-driven online generalized multiscale finite element methods, *J. Comput. Phys.*, **302** (2015), 176–190.
[18] E. T. Chung, Y. Efendiev and G. Li, An adaptive GMsFEM for high-contrast flow problems, *Journal of Computational Physics*, **273** (2014), 54–76.
[19] P. G. Ciarlet, *The Finite Element Method for Elliptic Problems*, volume 40. Siam, 2002.
[20] B. Cockburn, J. Gopalakrishnan and R. Lazarov, Unified hybridization of discontinuous galerkin, mixed, and continuous galerkin methods for second order elliptic problems, *SIAM Journal on Numerical Analysis*, **47** (2009), 1319–1365.
[21] L. J. Durlofsky, Numerical calculation of equivalent grid block permeability tensors for heterogeneous porous media, *Water Resour. Res.*, **27** (1991), 699–708.
[22] W. E and B. Engquist, Heterogeneous multiscale methods, *Comm. Math. Sci.*, **1** (2003), 87–132.
[23] Y. Efendiev and J. Galvis, Coarse-grid multiscale model reduction techniques for flows in heterogeneous media and applications, Chapter of *Numerical Analysis of Multiscale Problems, Lecture Notes in Computational Science and Engineering*, **83** (2012), 97–125.
[24] Y. Efendiev, J. Galvis and T. Hou, Generalized multiscale finite element methods, *Journal of Computational Physics*, **251** (2013), 116–135.
[25] Y. Efendiev, J. Galvis, S. Ki Kang and R. D. Lazarov, Robust multiscale iterative solvers for nonlinear flows in highly heterogeneous media, *Numer. Math. Theory Methods Appl.*, **5** (2012), 359–383.
[26] Y. Efendiev, J. Galvis, G. Li and M. Presho, Generalized multiscale finite element methods. Oversampling strategies, *International Journal for Multiscale Computational Engineering*, accepted, **12** (2014), 465–484.
[27] Y. Efendiev, J. Galvis and X. H. Wu, Multiscale finite element methods for high-contrast problems using local spectral basis functions, *Journal of Computational Physics*, **230** (2011), 937–955.
[28] Y. Efendiev and T. Hou, *Multiscale Finite Element Methods: Theory and Applications*, Springer, 2009.
[29] Y. Efendiev, T. Hou and V. Ginting, Multiscale finite element methods for nonlinear problems and their applications, *Comm. Math. Sci.*, **2** (2004), 553–589.
[30] Y. Efendiev and A. Pankov, Numerical homogenization and correctors for nonlinear elliptic equations, *SIAM J. Appl. Math.*, **65** (2004), 43–68.
[31] Y. Efendiev, J. Galvis, M Presho and J. Zhou, A multiscale enrichment procedure for nonlinear monotone operators, *ESAIM: Mathematical Modelling and Numerical Analysis*, **48** (2014), 475–491.
[32] Y. Efendiev, R. Lazarov, M. Moon and K. Shi, A spectral multiscale hybridizable discontinuous Galerkin method for second order elliptic problems, *Computer Methods in Applied Mechanics and Engineering*, **292** (2015), 243–256.
[33] J. Galvis and Y. Efendiev, Domain decomposition preconditioners for multiscale flows in high-contrast media, *Multiscale Model. Simul.*, **8** (2010), 1461–1483.

[34] J. Galvis and Y. Efendiev, Domain decomposition preconditioners for multiscale flows in high contrast media: reduced dimension coarse spaces, *Multiscale Model. Simul.*, **8** (2010), 1621–1644.
[35] R. Glowinski and A. Marroco, Sur l'approximation, par éléments finis d'ordre un, et la résolution, par pénalisation-dualité d'une classe de problèmes de dirichlet non linéaires, *Revue française d'automatique, informatique, recherche opérationnelle. Analyse numérique*, **9** (1975), 41–76.
[36] P. Henning, Heterogeneous multiscale finite element methods for advection-diffusion and nonlinear elliptic multiscale problems, *Münster: Univ. Münster, Mathematisch-Naturwissenschaftliche Fakultät, Fachbereich Mathematik und Informatik (Diss.). ii*, (2011), page 63.
[37] P. Henning and M. Ohlberger, Error control and adaptivity for heterogeneous multiscale approximations of nonlinear monotone problems, *Discrete and Continuous Dynamical Systems-Serie S. Special Issue on Numerical Methods based on Homogenization and Two-Scale Convergence*, **8** (2015), 119–150.
[38] T. J. R. Hughes, Multiscale phenomena: Green's functions, the Dirichlet-to-Neumann formulation, subgrid scale models, bubbles and the origins of stabilized methods, *Computer Methods in Applied Mechanics and Engineering*, **127** (1995), 387–401.
[39] T. J. R. Hughes, G. Feijoo, L. Mazzei and J. Quincy, The variational multiscale method—a paradigm for computational mechanics, *Comput. Methods Appl. Mech. Engrg.*, **166** (1998), 3–24.
[40] T. J. R. Hughes and G. Sangalli, Variational multiscale analysis: the fine-scale Green's function, projection, optimization, localization, and stabilized methods, *SIAM Journal on Numerical Analysis*, **45** (2007), 539–557.
[41] V. V. Jikov, S. M. Kozlov and O. A. Oleinik, *Homogenization of Differential Operators and Integral Functionals*, Springer-Verlag, Berlin, 1994.
[42] J. L. Lions, D. Lukkassen, L. E. Persson and P. Wall, Reiterated homogenization of nonlinear monotone operators, *Chinese Annals of Mathematics*, **22** (2001), 1–12.
[43] P. Ming and P. Zhang, et al., Analysis of the heterogeneous multiscale method for elliptic homogenization problems, *Journal of the American Mathematical Society*, **18** (2005), 121–156.
[44] G. Nguetseng and H. Nnang, Homogenization of nonlinear monotone operators beyond the periodic setting, *Electr. J. of Diff. Eqns*, **36** (2003), 1–24.
[45] H. Owhadi, L. Zhang and L. Berlyand, Polyharmonic homogenization, rough polyharmonic splines and sparse super-localization, *ESAIM: Mathematical Modelling and Numerical Analysis*, **48** (2014), 517–552.
[46] A. A. Pankov, *G-convergence and Homogenization of Nonlinear Partial Differential Operators*, volume 422. Mathematics and its Applications, 422. Kluwer Academic Publishers, Dordrecht, 1997.
[47] G. Papanicolau, A. Bensoussan and J.-L. Lions, *Asymptotic Analysis for Periodic Structures*, Elsevier, 1978.
[48] M. Presho and S. Ye, Reduced-order multiscale modeling of nonlinear p-Laplacian flows in high-contrast media, *Computational Geosciences*, **19** (2015), 921–932.
[49] X. H. Wu, Y. Efendiev and T. Y. Hou, Analysis of upscaling absolute permeability, *Discrete and Continuous Dynamical Systems, Series B.*, **2** (2002), 185–204.
[50] E. Zeidler, *Nonlinear Functional Analysis and Its Applications: III: Variational Methods and Optimization*, Springer-Verlag, New York, 1985.

Received January 2016; revised October 2016.

E-mail address: eric.t.chung@gmail.com
E-mail address: efendiev@math.tamu.edu
E-mail address: shike1983@gmail.com
E-mail address: yes.tamu2012@gmail.com